Prestack Depth Migration with the Gabor Transform

Yongwang Ma*
University of Calgary, Calgary, Alberta, Canada
yongma@ucalgary.ca

and

Gary Margrave
University of Calgary, Calgary, Alberta, Canada

Abstract

Summary

Wavefield extrapolation by spatially variable phase shift is currently a migration tool of importance. In this paper, we present a new prestack seismic migration algorithm using the Gabor transform with application to the Marmousi acoustic dataset. The imaging results show a very promising depth imaging algorithm, which is competitive with the best depth imaging algorithms.

The Gabor depth imaging algorithm approximates generalized phase-shift-plus-interpolation (GPSPI) wavefield extrapolation using a Gabor, or windowed Fourier, transform to localize the wavefield. The key to an efficient algorithm is to develop an adaptive windowing scheme that only localizes the wavefield as required by the lateral velocity variation. If there is no lateral velocity variation then no localization (windowing) is required. When velocity varies rapidly, then many, relatively narrow, windows are required for accurate wavefield extrapolation. We present the details of an adaptive windowing method that has a controlled phase error. Programs have been coded with the adaptive windowing algorithm, which substantially reduces the computational burden in wavefield extrapolation when compared to the full GPSPI integral. We will illustrate the performance of this algorithm with images from prestack depth migration of the Marmousi dataset.

Introduction

Migration with Gazdag (1978) phase shift method can only accommodate constant lateral velocity in any depth step, which is unrealistic for many practical applications, where velocity structures are often heterogeneous with strong lateral velocity fluctuations. To address lateral velocity variations in phase-shift wavefield extrapolations, phase shift plus interpolation (PSPI) was proposed by Gazdag and Sguazzero (1984) using a set of reference (laterally homogeneous) velocities to calculate the corresponding extrapolated wavefields; the final extrapolated wavefields are obtained by interpolating with specific velocities corresponding to certain lateral positions. Stoffa et al (1990) gave an alternative extrapolation algorithm, split-step Fourier migration, dealing with lateral velocity variation while keeping the advantages of the phase-shift method, i.e., accuracy and efficiency. Other phase-shift wavefield extrapolation methods such as `phase-screen propagator' (Wu and Huang, 1992; Roberts et al., 1997; Rousseau and de Hoop, 2001; Jin et al., 2002) also provide for

accurate imaging with abrupt velocity variations in such geological settings as salt-dome environments. Margrave and Ferguson (1999) used a nonstationary phase shift (NSPS) method and a generalized phase shift plus interpolation (GPSPI) to improve migration results, where wavefield extrapolations were done totally in the Fourier domain using arbitrary velocity variations. Our wavefield extrapolation method follows Jin and Wu (1998) and approximates GPSPI with a Gabor extrapolator. We also have control over speed and accuracy of Gabor wavefield extrapolations with the help of the adaptive windowing algorithm by Grossman et al., (2002). In the following sections, we will demonstrate the adaptive Gabor wavefield extrapolation algorithm and some imaging results created by these algorithms.

Gabor Wavefield Extrapolation Theory

The Gabor transform

The continuous Gabor transform pair is written as (following Margrave and Lamoureux (2001))

$$V_g s(x_T', k_T) = \int_{\Re} s(x_T) g(x_T - x_T') \exp(-i x_T k_T) dx_T \qquad (1)$$

and

$$s(x_T) = \int_{\Re^2} V_g s(x_T', k_T) \gamma(x_T - x_T') \exp(i x_T k_T) dk_T dx_T', \qquad (2)$$

where x_T denotes transverse coordinates (e.g., $x_T = x$ in 1D, $x_T(x, y)$ in 2D), $s(x_T)$ is the input signal, $V_g s(x_T', k_T)$ is the Gabor spectrum of $s(x_T)$, $g(x_T - x_T')$ is an analysis windowing function with its centre at x'_T, $\gamma(x_T - x_T')$ is a synthesis windowing function, and k_T is the coordinate in the wavenumber domain corresponding to x_T, $\Re$ denotes real domain for integrations. Equation (1) is in fact a Fourier transform of a windowed version of signal x_T.

Equation (1) is used to calculate the Gabor spectrum of $s(x_T)$; in order to recover the original signal $s(x_T)$ from its Gabor spectrum $V_g s(x_T', k_T)$, analysis and synthesis windows must satisfy

$$\int_{\Re} g(x_T) \gamma(x_T) dx_T = 1 \qquad (3)$$

(Margrave and Lamoureux, 2001), which is called a partition of unity (POU). The analysis windows could be any kind of mathematical functions. However, in our wavefield extrapolation applications, we choose functions with a localization property. In this way, we may represent our wavefield extrapolator depending on local velocities with a small error. Gaussian windows are good candidates, and we have chosen them for this paper. We also choose the synthesis window as unity, that is, we do no localization in the synthesis process.

Wavefield extrapolation with the Gabor transform

The generalized phase shift plus interpolation (GPSPI) wavefield extrapolation is formulated as (Margrave and Ferguson, 1999; Margrave et al., 2004)

$$\psi_P(x_T, z+\Delta z, \omega) = \int_{\Re} \hat{\psi}(k_T, z, \omega)\hat{W}(k_T, x_T, \Delta z)\exp(-ik_T x_T)dx_T\,, \tag{4}$$

where

$$\hat{W}(k_T, x_T, \Delta z) = \exp(ik_z(v(x_T))\Delta z)\,, \tag{5}$$

$$k_T(v(x_T)) = \begin{cases} \sqrt{\dfrac{\omega^2}{v^2(x_T)} - {k_T}^2}, & \dfrac{\omega^2}{v^2(x_T)} > {k_T}^2 \\ i\sqrt{{k_T}^2 - \dfrac{\omega^2}{v^2(x_T)}}, & \dfrac{\omega^2}{v^2(x_T)} < {k_T}^2, \end{cases} \tag{6}$$

Δz is the step size of extrapolation in z (vertical) direction, ω is temporal frequency and $v(x_T)$ denotes lateral velocities along a slab with thickness Δz. Equation (4) extrapolates wavefields at depth z down to depth $z+\Delta z$ in the frequency-wavenumber domain.

To develop a Gabor approximation to equation (4), we introduce the approximation

$$\hat{W}(k_T, x_T, \Delta z) \approx \sum_{j\in Z} \Omega_j(x_T) S_j(x_T) \hat{W}_j(k_T, \Delta z)\,, \tag{7}$$

$$\sum_{j\in Z} \Omega_j(x_T) = 1\,, \tag{8}$$

where Z denotes integer collection, Ω_j is a family of windows forming a POU (refer to equations (8)), the discrete form of POU), $S_j(x_T)$ is a split-step Fourier operator for phase correction in the Gabor imaging, $\hat{W}_j(k_T, \Delta z)$ is a wavefield extrapolator with reference velocities v_j, which are

$$S_j(x_T) = \exp\left(i\omega\Delta z\left(\frac{1}{v(x_T)} - \frac{1}{v_j}\right)\right), \tag{9}$$

$$\hat{W}_j(k_T, \Delta z) = \exp\left(ik_z(v_j)\Delta z\right) \tag{10}$$

and

$$v_j = \frac{\int_{\Re} \Omega_j(x_T) v(x_T) dx_T}{\int_{\Re} \Omega_j(x_T) dx_T}\,, \tag{11}$$

respectively. Notice that in equation (10), k_z is still calculated with equation (6), using the reference velocity v_j corresponding to a specific window Ω_j (see equation (11)) instead of $v(x_T)$. Using approximate wavefield extrapolator (7) in (4) gives

$$\psi_P(x_T, z+\Delta z, \omega) = \sum_{j\in Z} \Omega_j(x_T) S_j(x_T) \int_{\Re} \hat{\psi}(k_T, z, \omega)\hat{W}_j(k_T, \Delta z)\exp(-ik_T x_T)dx_T\,. \tag{12}$$

Equation (12) specifies our Gabor wavefield extrapolator.

Gabor wavefield extrapolation with adaptive windowing method

If analysis windows in Gabor wavefield extrapolations are uniformly distributed along the lateral dimensions, we will, in most circumstances, have excessive redundancy in computations. That is, the algorithm without adaptive windowing usually calculates more windowed Fourier transforms than it requires. For example, we know that for homogeneous media, we only need one window instead of many, where the GPSPI method degenerates into Gazdag (1978) Fourier migration (phase shift with constant velocity) in laterally homogeneous media. If the lateral velocity structures in a slab are not extremely inhomogeneous, we can use fewer windowed Fourier transforms in wavefield extrapolations than we do in rapidly varying velocity models. Adaptive windowing algorithms are suggested to deal with different types of lateral velocity structures met in Gabor wavefield extrapolations.

At this time, we use the Grossman et al. (2002) algorithm, which uses lateral velocity gradients to determine the number of windows needed in wavefield extrapolations.

Imaging the acoustic marmousi velocity structures with the Gabor extrapolator

The Marmousi synthetic data set has been widely used as a benchmark for testing depth imaging algorithms. The Marmousi velocity profile used in our depth imaging is shown in Figure 1 (a). In the Marmousi synthetic data set, we have 240 shot records, each of which has 96 traces, with time extending to about 2.9 seconds. For each shot record, there are 241 extrapolation steps with step size $\Delta z = 12.5$ meters.

Before we discuss the imaging results, we explain the parameter used in the adaptive windowing algorithm. We call this parameter `threshold', which is used to set the threshold in terms of the relative velocity variation (related to the lateral velocity gradients). For example, when threshold = 5, we mean that 1/5=20% of the mean velocity in the current window is set as the threshold; if velocity difference between the mean velocity of the current window and that of the next neighbouring window along the lateral dimension exceeds this threshold, we will not merge the next window into the current one. Otherwise, we do. That is, if the difference between the mean velocity of the current window's and that of the next one is smaller than the threshold set by `threshold', the next window is merged with the current window and the new combined window works as the `current' window. If not, we will leave the current window as it is and acquire the next as the `current' window, and repeat the process until we reach the edge of the lateral dimension. For mathematical details of the algorithm, see Grossman et al. (2002). If `threshold' is smaller, fewer windows will be used, and vise versa.

In imaging results Figure 1 (b) and (c), we used a threshold of 5. These are the cases in the Marmousi imaging with the most modest number of windows assigned by the adaptive windowing algorithm. We see that both are no better than the image in Figure 1 (d), where a threshold of 10 is used. Looking at the fault regions and the bottom part of the images in Figure 1 and examining the target reservoir, from 6000 m to 7500 m at about depth 2500 m; we can see that the reservoir is adequately imaged in (d), but not in (b) and (c). We conclude that more windows means better imaging results, but more expensive to calculate them. So with this parameter (threshold) we can

control the quality (accuracy) of the Gabor imaging. i.e., we have freedom to trade between accuracy and efficiency in the Gabor depth imaging.

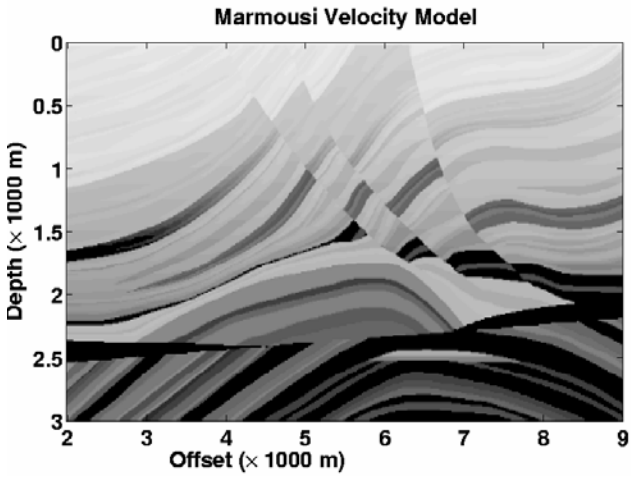

(a) Marmousi Velocity Model

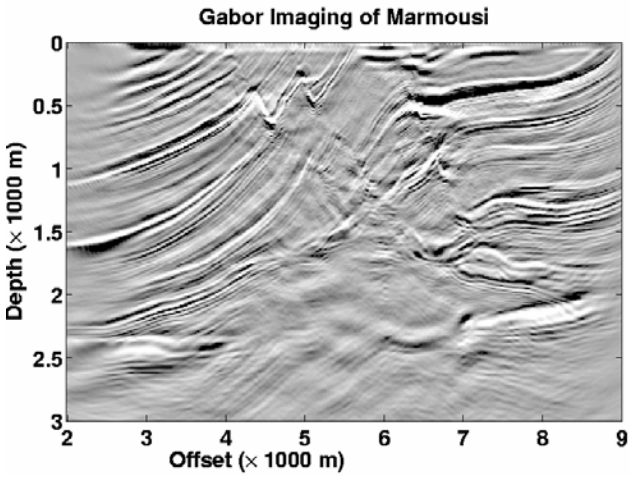

(b) Gabor Imaging without Split-step

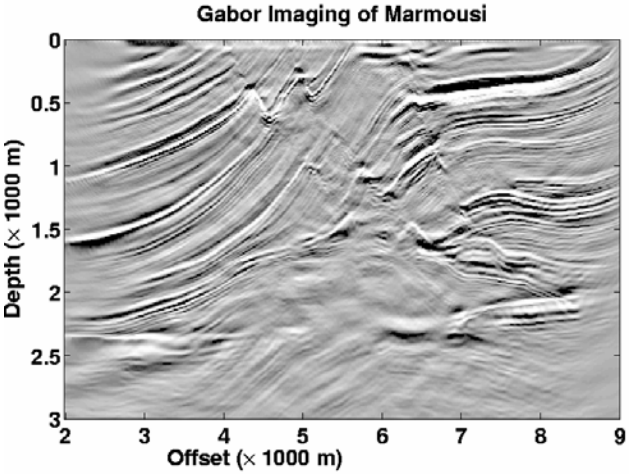

(c) Gabor Imaging with Split-step

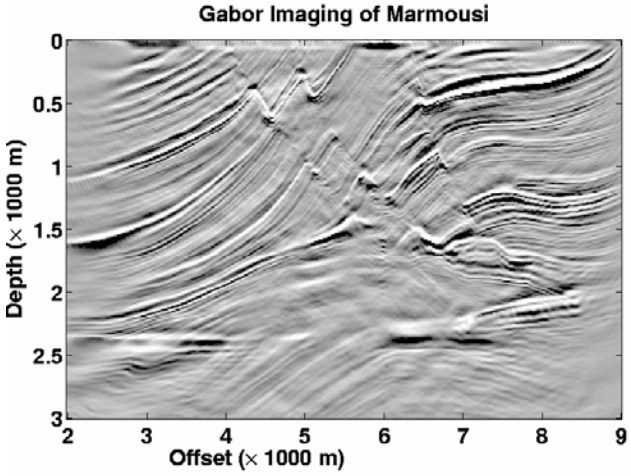

(d) Gabor Imaging with Split-step

Figure 1. Marmousi Velocity Model and Gabor Imaging Results. (a) windowing parameter threshold=5 without the split-step Fourier operator to correct phases in wavefield extrapolation with the Gabor wavefield extrapolator; (b) windowing parameter threshold=5 with the split-step Fourier operator to correct phases in the Gabor wavefield extrapolation; (c) windowing parameter threshold=10 with the split-step Fourier phase corrections. We can see from these three imaging results that with more windows used, the imaging results are better (compare (b) and (c)), and that with the phase correction, the imaging results are also better (compare (c) and (d)). On the PC with a CPU of 3.0 GHz, for the Gabor imaging of Marmousi velocity model with threshold=5, the CPU time is about 38 hours; if threshold=10 is used, CPU time will nearly double.

Figure 1 (b) and (c) are used to show how the split-step Fourier correction plays an important role in the Gabor depth imaging. Figure 1 (b) shows the Gabor imaging result without the split-step Fourier correction; Figure 1 (c) shows the result with the split-step Fourier correction. Both imaging results are calculated with the same windowing parameter, threshold=5, which means there is no imaging difference caused by the adaptive windowing. Without the split-step Fourier operator to correct phase in Gabor extrapolations, the imaging result is very poor compared to the one with the split-step operator. Examining Figure 1 (b) and (c) in the lower parts of the images, we can nearly see the imaged reservoir in (c) but not in (b).

To see how the adaptive windowing algorithm works in the Marmousi velocity model, in Figure 2 we show `windows versus the depth and the lateral coordinates (offsets)' corresponding to the dimensions of the Marmousi velocity model used in the Gabor imaging. The figure is created with the Gabor imaging process with a threshold of 20 (a finer windowing scheme); the corresponding Gabor depth imaging result is shown in Figure 3 (a), to be compared to the image generated by the FOCI (Figure 3 (b)).

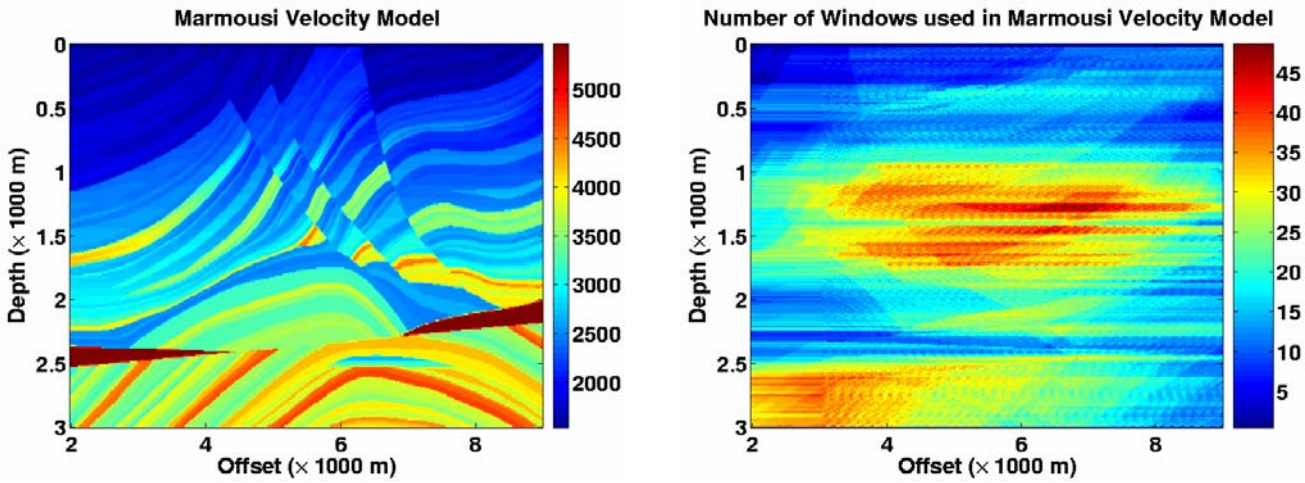

(a) The colour-coded Marmousi Velocity Model

(b) Number of Windows used in Marmousi Velocity Model

Figure 2. Windowing Marmousi Velocity Model with the Adaptive Windowing Algorithm. In (a), the units of the scale on the right are in m/s; in (b), the units of the scale on the right are in number of windows. Note that the transverse coordinates in (b) is not the true coordinates. The figure in (b) consists of 240 columns of `windows versus depth'. These columns are created during the shot migrations. Each of these 240 columns `windows versus depth' corresponding to a velocity `piece' adapted from the whole Marmousi velocity model used for a single shot migration. We put the true transverse coordinates into the figure to make it roughly comparable with the transverse coordinates in the velocity model (a) to see how the windows are distributed.

To show how well the Gabor extrapolator works, we use a FOCI (Margrave et al., 2004) Marmousi imaging result to compare with the Gabor Marmousi imaging result (see Figure 3 (a) and (b)). We see that, overall, the Gabor imaging algorithm gives a very good imaging result for the Marmousi velocity structures. Compared with the FOCI imaging result, the Gabor imaging method yields a very clear image of the Marmousi velocity model, though the FOCI seems to give more detailed and enhanced structural information in those over-thrust regions. The Gabor extrapolator may do as well as the FOCI in these regions with a more detailed windowing scheme. i.e., we can use more windows to get images that are comparable with the FOCI in those over-thrust regions, but the processing time will increase. In the lower part of Marmousi model, especially, the region of the anticline enclosing the target reservoir, both imaging methods do good jobs. The Gabor method creates clearer image just above the anticline than the FOCI does, while the FOCI images better inside the anticline. The Gabor extrapolator is slower than the FOCI for comparable results. Nevertheless, we have a hope to improve the accuracy and speed of imaging with the Gabor extrapolator by using some new adaptive windowing algorithms and different window sets.

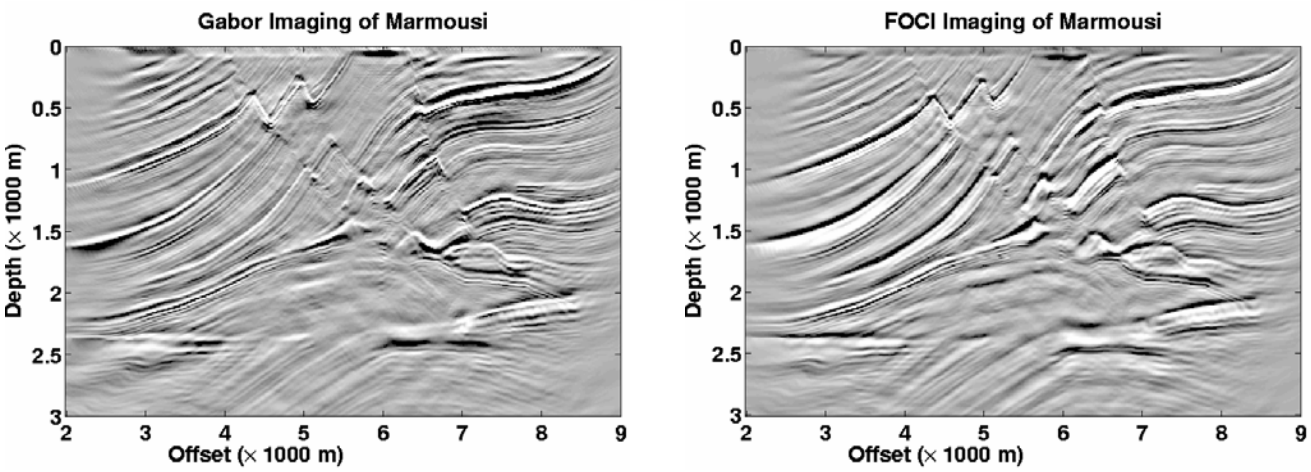

(a) Imaging with the Gabor Extrapolator **(b) Imaging with the FOCI**

Figure 3. Marmousi Imaging Results. (a) The Gabor imaging result with threshold=20 in (a) was created by a PC (3 GHz CPU) in about 112 hours; (b) FOCI imaging result runs on a common PC for about 20 hours.

Conclusions

The Gabor extrapolator is a very promising imaging tool in seismic depth migration. The Gabor imaging results have shown that we can get accurate depth images for complicated velocity structures such as the Marmousi acoustic velocity model, which is a solid basis for further research and exploration of the new imaging algorithm. The Gabor extrapolator can be used to image velocity structures as accurately as we may require. Computation (imaging) speed has been highly improved when the adaptive windowing algorithm is integrated into the Gabor wavefield extrapolation.

Acknowledgments

We would like to show our thanks to the sponsors of the CREWES project and the POTSI project; we are also grateful for all the financial and other supports from NSERC, PIMS, MITACS.

References

Gazdag, J., 1978, Wave equation migration with the phase-shift method: Geophysics, **43**, No. 7, 1342-1351

Gazdag, J., and Sguazzero, P., 1984, Migration of seismic data by phase shift plus interpolation: Geophysics, **49**, No. 2, 124-131.

Grossman, J. P., Margrave, G. F., and Lamoureux, M. P., 2002, Fast wavefield extrapolation by phase-shift in the nonuniform Gabor domain: CREWES Research Report, **14**.

Jin S., and Wu, R., 1998, Depth migration using the windowed generalized screen propagators: SEG Expanded Abstracts, **17**, 1843.

Jin, S., Xu, S., and Mosher, C. C., 2002, Migration with a local phase screen propagator: SEG Expanded Abstracts, **21**, 1164.

Margrave, G. F., Al-Saleh, S. M., Geiger, H. D., and Lamoureux, M. P., 2004, The FOCI algorithm for seismic depth migration: CREWES Research Report, **16**.

Margrave, G. F., and Ferguson, R. J., 1999, Wavefield extrapolation by nonstationary phase shift: Geophysics, **64**, No. 4, 1067-1078

Margrave, G. F., and Lamoureux, M. P., 2001, Gabor deconvolution: CREWES Research Report, **13**.

Roberts, P., Huang, L., Burch, C., Fehler, M., and Hildebrand, S., 1997, Prestack depth migration for complex 2D structure using phase-screen propagators: SEG Expanded Abstracts, **16**, 1982.

Rousseau, J., and de Hoop, M. V., 2001, Modeling and imaging the scalar generalized-screen algorithms in isotropic media: Geophysics, **66**, 1551-1568.

Stoffa, P. L., Fokkema, J. T., de Luna Freire, R. M., and Kessinger, W. P., 1990, Split-step Fourier migration: Geophysics, **55**, 410-421.

Wu, R., and Huang, L., 1992, Scattered calculation in heterogeneous media using a phase-screen propagator: SEG Expanded Abstracts, **11**, 1289.